Cell

Molecular Architecture and Functional Model of the Complete Yeast ESCRT-I Heterotetramer

Michael S. Kostelansky,[1] Cayetana Schluter,[2] Yuen Yi C. Tam,[2] Sangho Lee,[1,3] Rodolfo Ghirlando,[1] Bridgette Beach,[1] Elizabeth Conibear,[2] and James H. Hurley[1,*]
[1] Laboratory of Molecular Biology, National Institute of Diabetes and Digestive and Kidney Diseases, National Institutes of Health, U. S. Department of Health and Human Services, Bethesda, MD 20892, USA
[2] Centre for Molecular Medicine and Therapeutics, Child and Family Research Institute, Department of Medical Genetics, University of British Columbia, Vancouver, BC V5Z 4H4, Canada
[3] Present address: Department of Biological Science, Sungkyunkwan University, 300 Cheoncheon-dong, Suwon, Gyeonggi 440-746, Korea.
*Correspondence: hurley@helix.nih.gov
DOI 10.1016/j.cell.2007.03.016

SUMMARY

The endosomal sorting complex required for transport-I (ESCRT-I) complex, which is conserved from yeast to humans, directs the lysosomal degradation of ubiquitinated transmembrane proteins and the budding of the HIV virus. Yeast ESCRT-I contains four subunits, Vps23, Vps28, Vps37, and Mvb12. The crystal structure of the heterotetrameric ESCRT-I complex reveals a highly asymmetric complex of 1:1:1:1 subunit stoichiometry. The core complex is nearly 18 nm long and consists of a headpiece attached to a 13 nm stalk. The stalk is important for cargo sorting by ESCRT-I and is proposed to serve as a spacer regulating the correct disposition of cargo and other ESCRT components. Hydrodynamic constraints and crystallographic structures were used to generate a model of intact ESCRT-I in solution. The results show how ESCRT-I uses a combination of a rigid stalk and flexible tethers to interact with lipids, cargo, and other ESCRT complexes over a span of ~25 nm.

INTRODUCTION

The endosomal sorting complexes required for transport (ESCRTs) direct transmembrane proteins into inwardly budding vesicles at the multivesicular body (MVB) (Babst, 2005; Conibear, 2002; Hurley and Emr, 2006; Slagsvold et al., 2006). Sorting into the MVB pathway is a key step in the regulated degradation of transmembrane proteins in the lysosome or yeast vacuole. The ESCRT network is required for the downregulation of many cell surface receptors, for the delivery of resident hydrolases during lysosome and vacuole biogenesis, and for the production of exosomes from human cells (Katzmann et al., 2002). ESCRT complexes participate in the budding of HIV-1 and a number of other viruses (Demirov and Freed, 2004; Morita and Sundquist, 2004).

The ESCRT proteins were discovered as the products of class E vacuolar protein sorting (*VPS*) genes in the budding yeast *Saccharomyces cerevisiae* (Bowers and Stevens, 2005). Class E *vps* mutants have a characteristic enlarged cargo-rich compartment adjacent to the vacuole. Yeast class E *VPS* genes encode the subunits of at least four hetero-oligomeric protein complexes: the Vps27/Hse1 complex and ESCRT-I, -II, and -III (Bowers and Stevens, 2005; Hurley and Emr, 2006). Whereas monomeric ESCRT-III components are believed to assemble at the endosomal membrane, the other three complexes are assembled in the cytosol and cycle on and off membranes. Each of these soluble complexes contains specific ubiquitin binding domains that recognize ubiquitinated cargo proteins (Bilodeau et al., 2002; Hicke et al., 2005; Hurley et al., 2006; Katzmann et al., 2001; Shih et al., 2002; Slagsvold et al., 2005). Vps27/Hse1 (Katzmann et al., 2003) and ESCRT-II (Slagsvold et al., 2005; Teo et al., 2006) contain lipid binding domains that target these complexes to endosomal membranes. P(S/T)XP sequences in Vps27 bind to the ubiquitin E2 variant domain of the ESCRT-I subunit Vps23 (Bilodeau et al., 2003; Katzmann et al., 2003), whereas the C-terminal domain of the ESCRT-I subunit Vps28 binds to ESCRT-II (Kostelansky et al., 2006; Teo et al., 2006). Collectively, these interactions direct the assembly of the ESCRT network on endosomal membranes.

ESCRT-I contains the subunits Vps23, Vps28, and Vps37 and plays a central role in the MVB pathway (Katzmann et al., 2001). Human Vps23 (Tsg101) is one of a handful of ESCRT proteins whose knockdown by RNA interference almost completely blocks HIV budding

(Garrus et al., 2001). The structure and function of ESCRT-I has come under intense scrutiny, and the structures of many of its components have been determined. The N-terminal UEV domains of yeast and human Vps23 have been determined in complex with ubiquitin (Sundquist et al., 2004; Teo et al., 2004b) and, for the human case, with a PTAP motif peptide from HIV-1 (Pornillos et al., 2002). The C-terminal domain of Vps28, responsible for binding to ESCRT-II, is a four-helix bundle (Pineda-Molina et al., 2006).

The structure of a globular core complex comprising the C-terminal steadiness box of Vps23, the N-terminal half of Vps28, and the C-terminal half of Vps37 showed how the three subunits assemble together (Kostelansky et al., 2006; Teo et al., 2006). However, the structures and functions of the central region of Vps23 and the N-terminal half of Vps37, both conserved from yeast to man, have yet to be characterized. Furthermore, ESCRT-I isolated from yeast has an apparent molecular weight of 350 kDa as judged by gel filtration (Katzmann et al., 2001), yet near full-length recombinant ESCRT-I purified from *E. coli* has an apparent molecular weight of only ~200 kDa (Kostelansky et al., 2006; Teo et al., 2006). This discrepancy led to the question as to whether ESCRT-I in yeast oligomerizes or contains additional subunits.

Here we identify a fourth ESCRT-I subunit, Mvb12, and characterize the structure and function of the quaternary Vps23:Vps28:Vps37:Mvb12 ESCRT-I complex. The complete recombinant ESCRT-I complex migrates on gel filtration in a manner identical to native yeast ESCRT-I and has a 1:1:1:1 subunit stoichiometry. We determined the crystal structure of the core of the complete heterotetrameric complex, which includes a novel 130 Å-long stalk. The integrity of the stalk is essential for sorting MVB cargo. Hydrodynamic analysis of full-length and multiple truncation constructs was used in combination with crystal structures to determine the conformation of intact ESCRT-I in solution. The physical interactions of ESCRT-I with membranes were inventoried and used to model the structure of ESCRT-I bound to an endosomal membrane.

RESULTS

Mvb12 Is the Fourth Subunit of ESCRT-I

Genome-wide phenotypic profiling was used to identify mutants defective in the sorting of carboxypeptidase Y (CPY) (E.C., unpublished data). Known ESCRT-associated factors, including the *VPS4*-regulatory genes *VTA1* and *DID2*, and the Vps27/Hse1 component *HSEI*, were found in a cluster enriched for genes that encode endosome-localized proteins, including the ORF YGR206w (E.C., unpublished data), which was also identified in another screen for CPY sorting mutants (Bonangelino et al., 2002). Coclustering with ESCRT regulatory factors suggests this endosome-associated ORF, which is now known as Mvb12, could play a role in sorting at the MVB. *mvb12*Δ mutants have a weak CPY missorting phenotype compared to that of *vps4*Δ strains (Figure 1A). In wild-type cells, Mvb12-GFP was diffusely localized, with faint punctate staining (Figure 1B); however, in *vps4Δ* mutants, Mvb12-GFP was found in brighter puncta that colocalized with FM4-64, a characteristic of ESCRT components. *mvb12*Δ mutants also exhibited defects in MVB cargo sorting similar to those of ESCRT mutants (Figure 1C). The cargo proteins Ste3 and Sna3 largely failed to reach the vacuole lumen in *mvb12*Δ mutants and instead accumulated in aberrant MVB structures and at the vacuole-limiting membrane. Each *mvb12*Δ mutant phenotype was fully complemented by a *MVB12*-encoding plasmid. The strong Ste3 and Sna3 mislocalization phenotypes suggest that Mvb12 is important for sorting MVB cargo.

Mvb12 Is a Component of the ESCRT-I Complex

Because ESCRT complexes are recruited to the MVB in a stepwise fashion, the localization of Mvb12 in representative mutants provides a way to evaluate its association with a particular ESCRT complex. Mvb12 was found at the enlarged MVB in ESCRT-II (*vps22*Δ and *vps36*Δ) and ESCRT-III (*vps20*Δ) mutants, indicating that recruitment of Mvb12 is independent of these ESCRT complexes (Figures 1D and S1A). Mvb12 was diffusely localized in Vps27/Hse1 (*vps27*Δ) mutants and in mutants lacking two different components of ESCRT-I (*vps23*Δ and *vps37Δ*). The recruitment of Mvb12-GFP to FM4-64-labeled endosomes was completely blocked in either *vps27*Δ *vps4*Δ or *vps23*Δ *vps4*Δ double mutants and restored upon introduction of a complementing plasmid-borne copy of *VPS27* or *VPS23*, respectively (Figure 1B).

The physical interaction between Mvb12 and the ESCRT-I subunit Vps23 was tested by coimmunoprecipitation of tagged proteins from cell lysates. Mvb12 and Vps23 copurified efficiently, with immunoprecipitation of 80% of the cellular Vps23 resulting in the coprecipitation of a nearly equal proportion (70%) of cellular Mvb12 (Figure 1E; lane 3). These findings are consistent with the physical association of Mvb12 with ESCRT-I components in proteome-wide screens of yeast protein complexes (Gavin et al., 2006; Krogan et al., 2006). Unexpectedly, loss of the ESCRT-I subunit Vps28 resulted in an enhanced MVB recruitment of Mvb12, similar to that seen in ESCRT-II and -III mutants (Figure 1D). The copurification of Mvb12 and Vps23 required Vps37, but not Vps28 (Figure 1E; lanes 8–10). Mvb12 thus appears to associate with a stable, MVB-localized Vps23/37 subcomplex in *vps28*Δ mutants. Although ESCRT-I is found both in cytosol and membrane-bound pools, the amount of Mvb12 that coprecipitated with Vps23 was unchanged in *vps27*Δ mutants, in which ESCRT-I is entirely cytosolic, compared to *vps4*Δ strains, where it is primarily endosome localized (Figure 1E; lanes 4 and 5). This indicates that Mvb12 does not preferentially associate with a specific subcellular fraction of ESCRT-I. Taken together, these data support the model that Mvb12 is an integral component of the ESCRT-I complex.

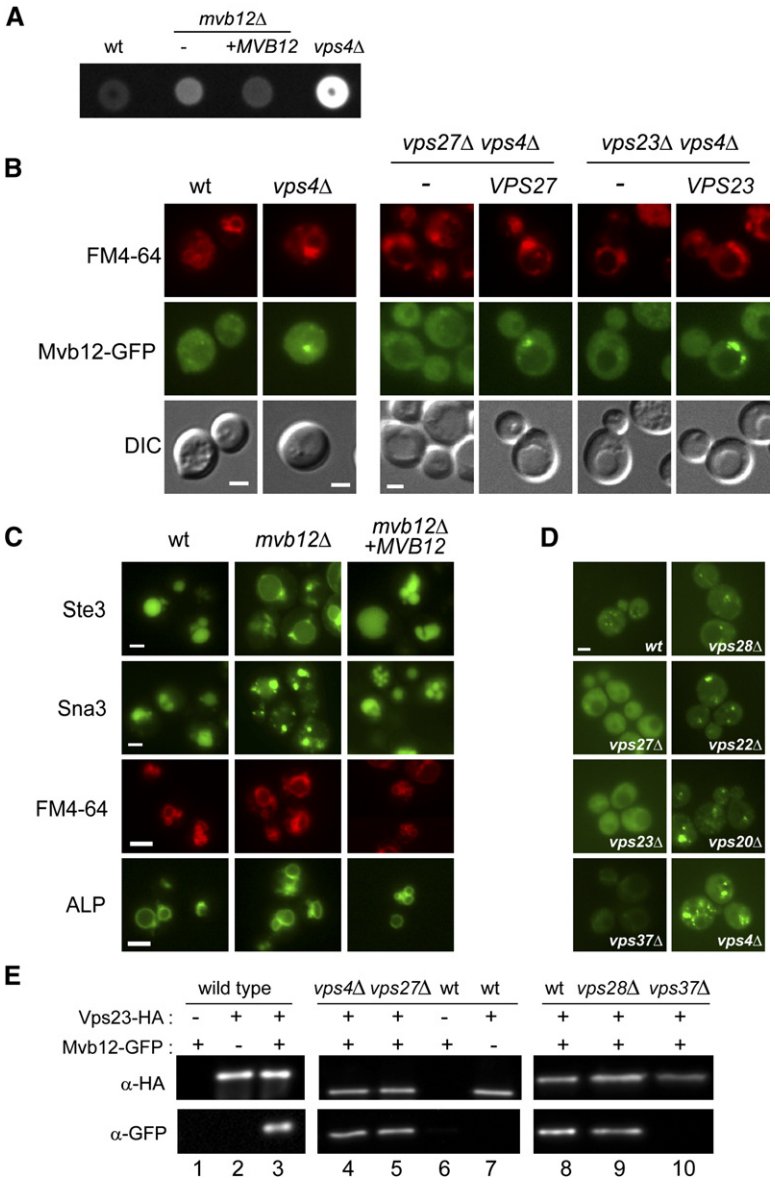

Figure 1. Identification of the Novel ESCRT-I Subunit Mvb12

(A) *mvb12* mutants exhibit a weak CPY-sorting defect. CPY missorting from wild-type, *vps4Δ*, or *mvb12Δ* strains with and without an *MVB12*-expressing plasmid (+*pMVB12*) was detected by colony overlay assay (Conibear and Stevens, 2002).

(B) Mvb12 is recruited to the endosome in *vps4Δ* mutants. *vps27Δvps4Δ* and *vps23Δvps4Δ* strains containing integrated Mvb12-GFP and plasmid-expressed *VPS27* and *VPS23,* or empty vector, were incubated with FM4-64 and viewed by double-label fluorescence microscopy.

(C) Fluorescence microscopy of wild-type and *mvb12Δ* strains containing Ste3-GFP, Sna3-GFP, or ALP-GFP plasmids together with a complementing *MVB12* plasmid or empty vector.

(D) Mvb12 recruitment does not require ESCRT-II or -III. The chromosomal copy of *MVB12* was tagged with GFP in wild-type, *vps27Δ*, *vps23Δ*, *vps37Δ*, *vps28Δ*, *vps22Δ*, and *vps20Δ* strains and visualized in live cells.

(E) Mvb12 is associated with ESCRT-I. Detergent extracts prepared from 20 OD_{600} units (lanes 1–7) or 100 OD_{600} (lanes 8–10) of wild-type or mutant strains expressing GFP-tagged Mvb12 and/or HA-tagged Vps23 were immunoprecipitated with anti-HA antiserum and analyzed by western blotting with anti-GFP and anti-HA mAbs. Loading of lanes 9 and 10 was 7.5× greater than lane 8 to compare relative levels of copurifying Mvb12-GFP despite differences in Vps23 stability. Bar = 2 μM.

Structure of the Heterotetrameric ESCRT-I Core Complex

The structure of a heterotetrameric core complex of ESCRT-I was determined at a nominal resolution of 2.7 Å (Figure 2A; Table S1). The heterotetrameric core ESCRT-I structure consists of a globular headpiece attached to an extended stalk (Figure 2B). The overall structure is 176 Å long. The headpiece is a flattened blade of 25 × 55 × 60 Å that corresponds to the ESCRT-I ternary core complex (Figures 2C–2E) (Kostelansky et al., 2006; Teo et al., 2006). The stalk is a cylinder of 20 Å diameter bent gently into a 130 Å long S-shaped curve. The headpiece includes portions of all four subunits, while the stalk contains regions of Vps23, Vps37, and Mvb12, but not Vps28 (Figures 2F–2H). Consistent with the finding that Mvb12 forms a subcomplex in vivo with Vps23 and Vps37, but not Vps28, the Mvb12:Vps28 interface buries a negligible amount of solvent accessible surface area, 68 $Å^2$ (Figure 4). By contrast, Mvb12 buries 1470 and 2318 $Å^2$, respectively, in its interfaces with Vps23 and Vps37. In total, Mvb12 buries a remarkable 42% of its solvent-accessible surface area in the complex, leaving no doubt that it is an integral core component of ESCRT-I.

The headpiece is built around three antiparallel two-helix hairpins (Figures 2C–2E) and superimposes well with the ternary core (rmsd of 0.8 Å for 193 Cα positions). Residues of Vps28 that correspond to α3 in the ternary core are disordered in this structure, while Vps28 helix α4 is in a completely different position than in the ternary core. Mvb12 contributes its N-terminal α1 helix to the headpiece. The headpiece contains a two-stranded antiparallel β sheet (Figure 2F), not present in the ternary

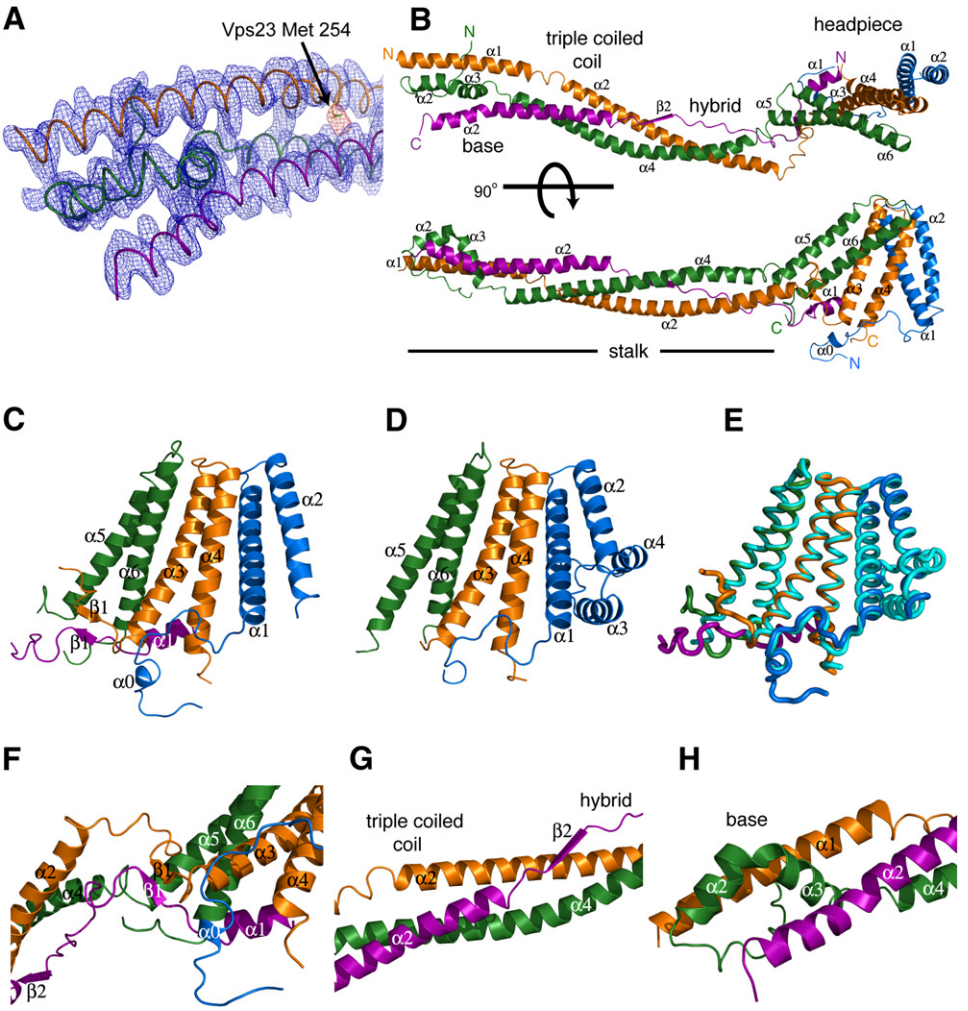

Figure 2. Structure of the ESCRT-I Heterotetramer Core

(A) Electron density from the density-modified experimental map (blue) contoured at 1.0 σ and from a Se anomalous difference Fourier contoured at 4.0 σ (yellow) overlaid on the refined structure in the region of the helix bundle at the distal end of the stalk.

(B) Structure of ESCRT-I, Vps23, orange, Vps28, blue, Vps37, green, Mvb12, purple.

(C–E) Structure of the headpiece in the heterotetramer, shown with (D) the previously determined trimeric core structure in the same orientation. The two structures are overlaid in (E) with the heterotetramer headpiece colored as in (C) and the trimer colored cyan.

(F) The headpiece contains a small β sheet near its junction with the stalk.

(G) The triple coiled coil is continued and stabilized by an unusual hybrid between a two-stranded coiled coil and an extended region of Mvb12.

(H) The helix bundle at the base of the stalk. Structural figures were generated with Pymol (http://www.pymol.org).

complex. Mvb12-β1 (residues 14–16) is antiparallel to Vps23 residues 317–319. This miniature β sheet connects the headpiece to the stalk.

The stalk is centered on four long α helices, two from Vps23, and one each from Vps37 and Mvb12 (Figures 2B, S2, and S3). The Vps23 α1 and α2 helices are nearly colinear and run the entire length of the stalk (Figure 2B). A short 3_{10} helix (residues 247–253) separates these two α helices. The α4 helix of Vps37 is nearly as long. Mvb12 contributes its α2 helix to the stalk (Figure 3A). These three long helices come together to form a triple coiled coil over part of their lengths (Figure 2G). Vps23 residues 254–265, Vps37 residues 89–106, and Mvb12 residues 43–61 form a triple coiled coil in which Vps23 and Vps37 are parallel and Mvb12 antiparallel. The triple coiled coil comprises the center of the stalk. Proximal to the headpiece, Vps23 α2 and Vps37 α4 form an unusual partnering (the "hybrid") with an extended portion of Mvb12, residues 18–39 (Figures 3C and 3D). Here Mvb12 contributes a series of hydrophobic residues to stabilize the groove between Vps23 and Vps37 (Figure 3D). At the base of the stalk, distal to the headpiece, helices α2 and α3 of Vps37 form a small four-helix bundle with the N terminus of Vps23 α1 and the C terminus of Mvb12 α2 (Figures 2H and 3A). The very N-terminal helix α1 of Vps37 is not part of the stalk at all. It is not directly associated with the rest of

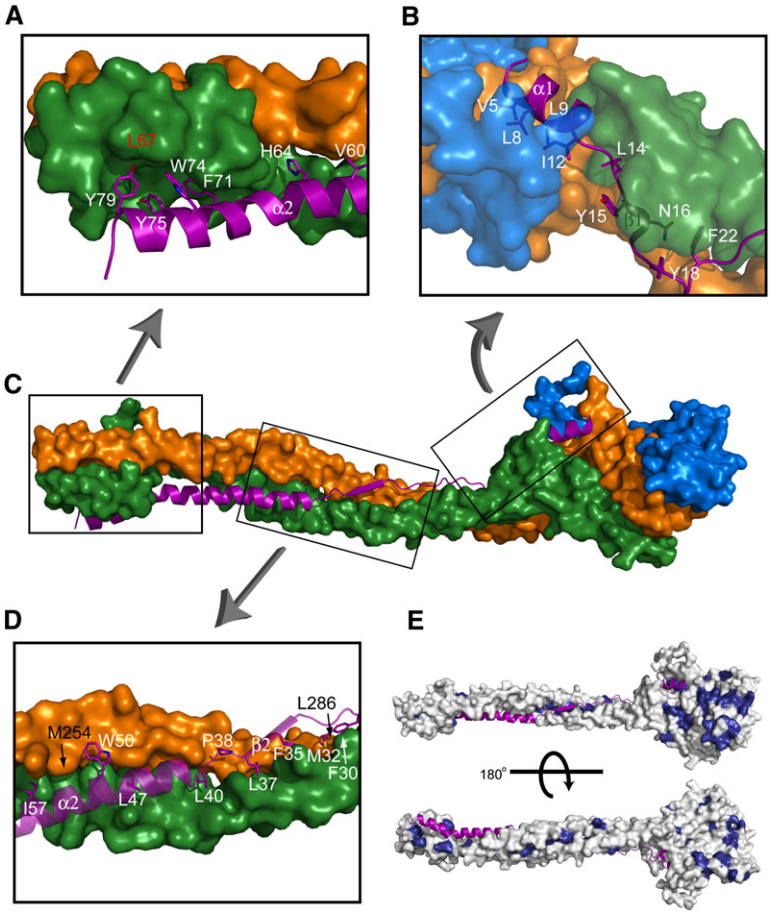

Figure 3. Interactions within the ESCRT-I Heterotetramer

(A, B, and D) Close ups of the interface of Mvb12 (purple ribbon and stick model) with Vps23, Vps28, and Vps37 (orange, blue, and green surfaces, respectively).

(C) Shows locations of the regions of the ESCRT-I heterotetramer highlighted in panels (A), (B), and (D). Mvb12 residues are labeled in white, while significant Vps23 residues are labeled in black and Vps37 residues in red.

(E) Surface depiction of the ESCRT-I heterotetramer showing in dark-blue residues highly conserved in orthologs of Vps23, Vps28, and Vps37. Mvb12 is depicted as a ribbon. The conservation of the Mvb12 interaction surface on the rest of the stalk suggests that there is a structural counterpart of Mvb12 in nonfungal species.

the protein and is apparently trapped in an ordered conformation due to lattice contacts. A well-ordered sulfate ion is bound in the stalk region by Vps37 His-71, His-73, and Gln-74, suggestive of a potential phospholipid interaction site. However, the overall electronegative character of the stalk argues against a direct interaction with membranes.

Stoichiometry and Solution Conformation of ESCRT-I

The full-length heterotetrameric ESCRT-I complex consisting of intact Vps23, Vps28, Vps37, and Mvb12 runs on gel filtration chromatography with an apparent molecular weight of 340 kDa (Figure 4B), identical within error to the 350 kDa previously reported for native ESCRT-I isolated from *S. cerevisiae* (Katzmann et al., 2001). Sedimentation equilibrium centrifugation analysis revealed that full-length ESCRT-I sample has an experimental molecular mass of 117 ± 4.6 kDa (Figure 4C and Table S2), as compared to a calculated molecular mass for a 1:1:1:1 heterotetramer of 108 kDa. The experimental molecular mass is consistent with a "monomeric" complex of n = 1.08 ± 0.04 and is inconsistent with any higher oligomeric structures.

The stoichiometry and solution conformation of intact ESCRT-I was characterized by sedimentation velocity experiments on intact heterotetrameric ESCRT-I and two truncated constructs (Figure 4A and Table S2). The frictional ratio of intact ESCRT-I, f/f_o, is 1.9 ± 0.1. Globular proteins have f/f_o values ranging from 1.05 to 1.35, whereas rod-like particles have f/f_o values of 3 and larger. The elongated shape of ESCRT-I in solution quantitatively predicts its elution volume on gel filtration chromatography (Figure S2). The solution conformations of the Vps23 UEV domain, the Vps28 C-terminal domain, and the Vps37 N-terminal helix were assigned on the basis of iterative modeling of the three experimental values for the Stokes radii R_H (Figure 4A). The best fit for the double-deletion construct was obtained by modeling the N terminus of Vps37 in a partially extended conformation (Figure 4D). The experimental Stokes radii rule out a "closed" conformation in which the UEV or Vps28 C-terminal domain contacts the core in solution. In the absence of Mvb12, the heterotrimeric UEV-domain deletion of ESCRT-I has an experimental Stokes radius R_H = 4.97 nm and a frictional ratio of 1.8, indicating ESCRT-I retains an extended structure. On the other hand, if the length and stability of the stalk were fully maintained in the absence of Mvb12, this would yield a calculated

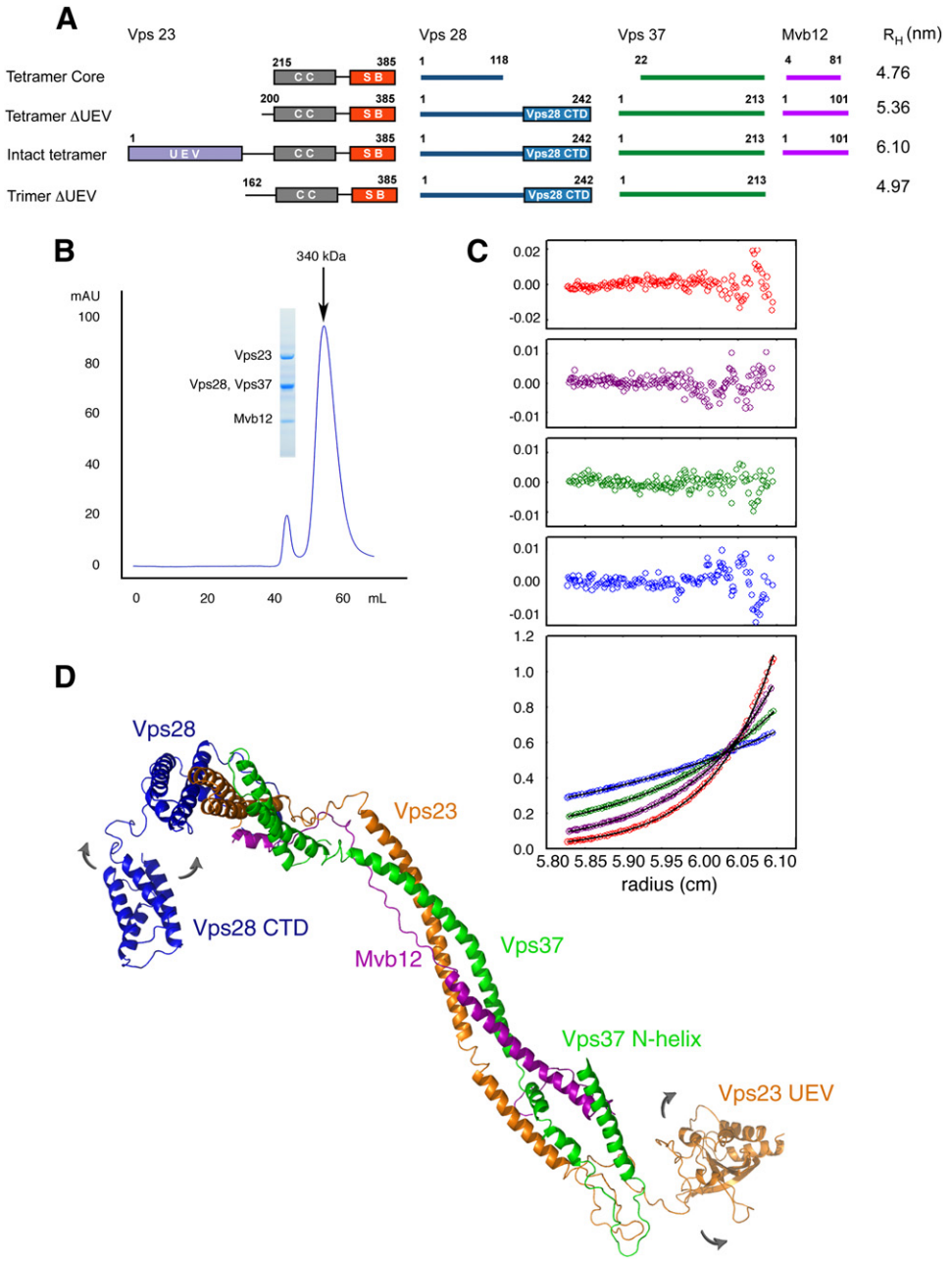

Figure 4. Stoichiometry and Solution Structure of the Complete ESCRT-I Complex

(A) Domain structure of full-length ESCRT-I and other constructs used in this study and their Stokes radii R_H as determined by analytical ultracentrifugation.

(B) Gel filtration of full-length ESCRT-I, monitored at 280 nm. The inset shows a Coomassie blue-stained SDS-PAGE gel of the peak fraction indicated.

(C) Sedimentation equilibrium profiles of full-length ESCRT-I plotted as a distribution of A_{280} versus r at equilibrium. Data were collected at 6 (blue), 8 (green), 10 (purple), and 12 (red) krpm at a loading A_{280} of 0.38 (alternate data points are shown). The solid lines show the best-fit global analysis in terms of a single ideal solute, with the corresponding residuals shown in the panels above the plot.

(D) Solution structural model of intact ESCRT-I. The curved arrows indicate that the Vps23 UEV and Vps28 C-terminal domain (CTD) are conformationally dynamic.

R_H = 5.45 nm for the heterotrimeric UEV-domain deletion construct. Thus, when Mvb12 is not present, the solution conformation of ESCRT-I is only modestly less extended than the intact complex.

The Stalk Is Important for the Function and Assembly of ESCRT-I

To test the role of the stalk in ESCRT-I function, mutations were engineered in Vps23, Vps37, and Mvb12.

Residues in the base, triple coiled coil, and hybrid regions of the stalk were altered alone and in combination. A spectrum of effects was observed in various mutants (Table S3). Some mutants, such as the combined triple coiled coil and hybrid region mutant *vps23*$^{M254D/L286D}$ (Figure S5), severely disrupted all ESCRT-I functions by blocking the assembly of the complex and destabilizing the subunits. Other mutations produced less drastic effects. We chose three representative alleles of this latter class for further study, *vps23*^{M254D} and *mvb12*$^{L47D/I57D}$ (triple coiled coil) and *vps37*^{L67D} (base). With the exception of reduced stability of Mvb12 in *vps37*^{L67D} strains, the different mutations had little if any effect on steady-state levels of the other subunits (Figure S1C). However, all three gave rise to defects in the sorting of the MVB cargos Ste3 and Sna3 (Figure 5A). Some labeling of both cargos was observed in the vacuolar lumen of the mutants, similar to that seen in *mvb12Δ* cells. Vps37^{L67D} and Vps23^{M254D} mutations also resulted in a CPY sorting defect at least as severe as that of *mvb12*Δ mutants, whereas little CPY was secreted from *mvb12*$^{L47D/I57D}$ mutants (Figure S1B; Table S3).

We examined the effect of each mutation on ESCRT-I membrane recruitment. Both Vps23^{M254D} and Mvb12$^{L47D/I57D}$ greatly reduced Mvb12 localization to the MVB in *vps4*Δ strains (Figure 5B). However, Mvb12$^{L47D/I57D}$ had little effect on the MVB localization of Vps23 in either wild-type cells or *vps4*Δ mutants (Figure 5C), suggesting this mutation reduces the assembly of Mvb12 into the ESCRT-I complex without disrupting the membrane association of ESCRT-I. In contrast, Vps37^{L67D} did not block the MVB association of either Mvb12 or Vps23 (Figures 5B and 5C).

Coimmunoprecipitation experiments were used to test the effect of each mutation on ESCRT-I assembly (Figures 5D–5F). The mutant complexes showed varying levels of stability during copurification from native cell extracts. Consistent with the in vivo localization data, Vps23^{M254D} and Mvb12$^{L47D/I57D}$ mutations had the greatest effect on the incorporation of Mvb12 into the complex. Vps23^{M254D} blocked the Vps23-Mvb12 interaction and reduced, but did not prevent, Vps23 binding to Vps37, whereas Mvb12$^{L47D/I57D}$ showed reduced binding to both Vps23 and Vps37. Vps37^{L67D}-containing complexes contained wild-type levels of Mvb12 and Vps23, in keeping with the MVB localization of both proteins.

These results indicate that the stalk contributes to the function of the ESCRT-I complex in vivo. CPY secretion of the *mvb12*$^{L47D/I57D}$ mutant was close to wild-type (Figure S1B), suggesting that perturbations of the stalk that do not disrupt CPY sorting can nevertheless lead to significant MVB cargo-sorting defects. Vps37^{L67D} assembled at near wild-type efficiency yet caused significant missorting of CPY, Ste3, and Sna3. Thus, the base of the stalk is less critical for assembly than the triple coiled coil or hybrid regions of the stalk, yet is equally important for cargo sorting.

Interactions of ESCRT-I with Model Membranes In Vitro

To investigate the physical basis for the binding of ESCRT-I to the endosomal membrane, we sought to define the interactions responsible for its binding to membranes in vitro. Full-length ESCRT-I bound to brain lipid and bound weakly to synthetic PI(3)P-containing vesicles (Figures 6A and 6B). No enhancement of binding was observed in PI(3)P-containing vesicles compared to generic brain lipid vesicles. No binding was observed in the Vps37 Δ1–21 construct, indicating that the basic N terminus of Vps37 is required for binding. ESCRT-II bound weakly to Folch lipids (Figure 6A), but strongly to PI(3)P-containing synthetic liposomes (Figure 6B), consistent with previous findings (Teo et al., 2006). ESCRT-I and ESCRT-II were mixed at a 1:1 ratio and found to bind weakly to Folch but strongly to PI(3)P-containing synthetic liposomes. These data show that ESCRT-I can bind weakly and nonspecifically to anionic lipids via the basic N terminus of Vps37. In contrast, ESCRT-I and ESCRT-II together bind strongly and specifically to a PI(3)P-containing model membrane. The triple complex of Vps23:Vps28:Vps37 Δ1–21 bound to roughly the same extent as intact ESCRT-I in the presence of ESCRT-II, indicating the loss of Mvb12 does not affect the assembly of a membrane-bound ESCRT-I/II complex (Figure 6C).

We developed an in vitro model MVB cargo based on Cps1, which is ubiquitinated at Lys-8 (Katzmann et al., 2001), 11 residues from the start of its transmembrane helix. A construct in which ubiquitin was fused to Cps1 residues 8–17 followed by a unique C-terminal Cys residue (Ub-Cps1[8–17]C) was covalently conjugated to liposomes (Figure 6D). These liposomes, but not control liposomes, bound to the ubiquitin-binding domains of Rabex-5 (Figure 6E). The ability of ESCRT-I, -II, and the ESCRT-I/-II complex to bind to PI(3)P-containing vesicles was not substantially enhanced by the model cargo, consistent with the low affinities of the ESCRT-I and -II ubiquitin-binding domains. To explore whether Mvb12 alters recruitment by Vps27, a "miniVps27" consisting of the PI(3)P-binding FYVE domain, the ubiquitin-binding ubiquitin-interacting motif domains, and the ESCRT-I-binding P(S/T)XP sequences was purified. MiniVps27 binds to PI(3)P-containing ubiquitin-Cps1-conjugated liposomes (Figure 6E), but does not bind to control PC:PE liposomes (data not shown). ESCRT-I binding to these liposomes was markedly enhanced by the presence of miniVps27 (Figure 6E), independent of the presence or absence of Mvb12. Thus Mvb12 does not appear to regulate the interaction of Vps27 and ESCRT-I in vitro, consistent with the absence of a structural interaction between Mvb12 and the Vps27-binding UEV domain of Vps23.

DISCUSSION

The results presented here essentially complete the structural description of yeast ESCRT-I. The presence of a 130 Å long stalk is the most dramatic new feature of the

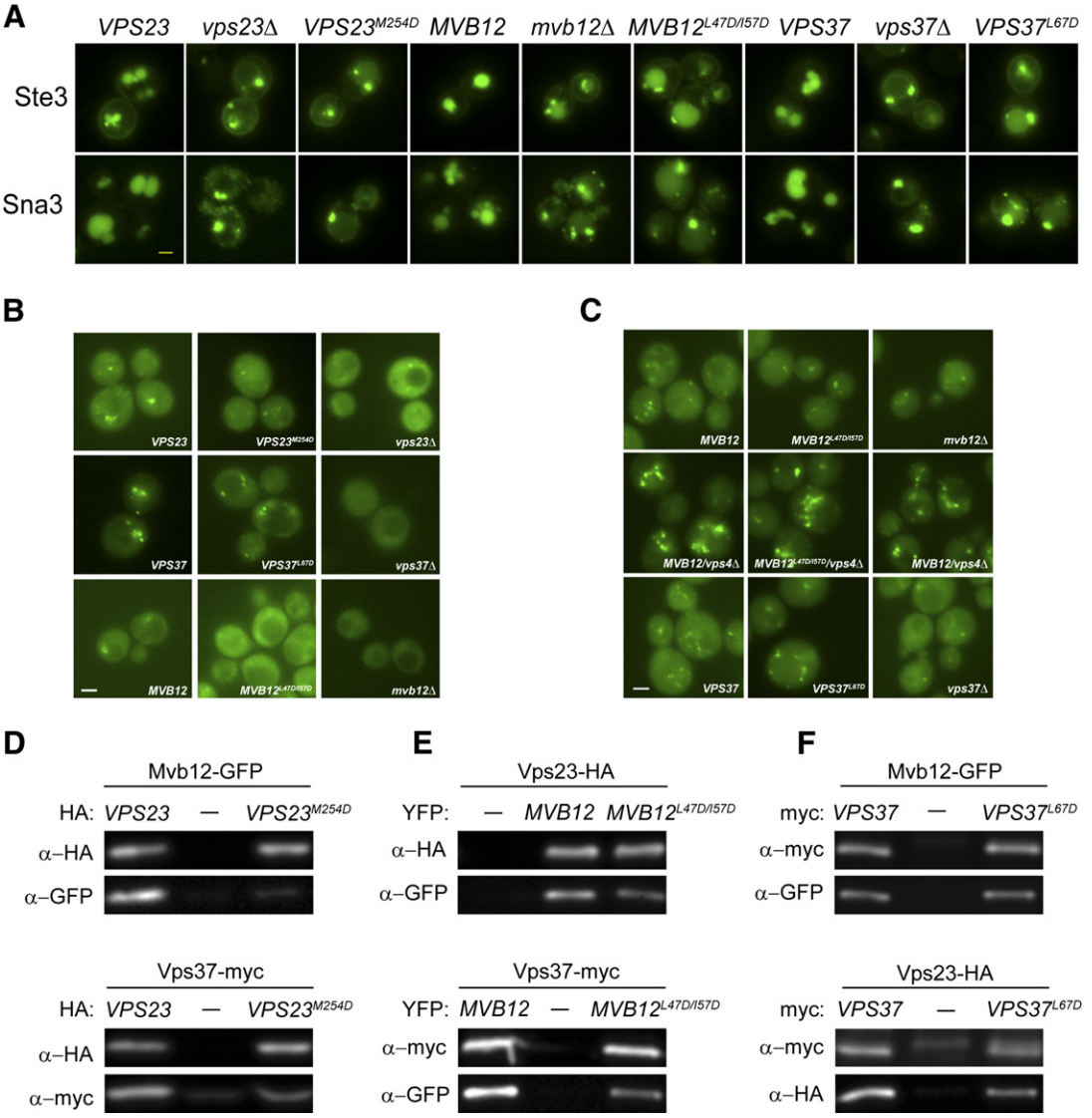

Figure 5. The Stalk Is Essential for ESCRT-I Function

(A) Ste3 and Sna3 sorting defects in stalk mutants. Plasmids expressing wild-type or mutant forms of *VPS23*, *MVB12*, or *VPS37* were introduced into *vps23Δ*, *mvb12Δ*, or *vps37Δ* strains expressing plasmid-encoded Ste3-GFP or Sna3-GFP, as indicated.

(B) Mvb12 localization depends on the integrity of the stalk. Wild-type or mutant forms of *VPS23* or *VPS37* were expressed from plasmids in *vps23Δvps4Δ* or *vps37Δvps4Δ* strains containing chromosomally integrated Mvb12-GFP, whereas plasmid-encoded wild-type and mutant forms of Mvb12-YFP were expressed in *mvb12Δvps4Δ* strains.

(C) Stalk mutants do not prevent Vps23 localization to the MVB. Wild-type or mutant forms of *VPS37* or *MVB12* were expressed from plasmids in *vps37*Δ, *mvb12*Δ, or *mvb12Δvps4Δ* strains containing chromosomally integrated Vps23-GFP.

(D–F) Stalk mutations have differential effects on ESCRT-I assembly. In (D), detergent extracts from *vps23Δ* mutants containing chromosomally tagged Mvb12-GFP (upper panels) or Vps37-13myc (lower panels) and plasmids for the expression of HA-tagged wild-type or mutant forms of Vps23 were subjected to immunoprecipitation with anti-HA antiserum (E) *mvb12Δ* mutants containing chromosomally tagged Vps23-6HA (upper panels) or Vps37-13myc (lower panels), and plasmid-borne wild-type or mutant forms of Mvb12-YFP were immunoprecipitated with either anti-HA (upper panels) or anti-myc (lower panels) antiserum. In (F), *vps37Δ* mutants containing chromosomally tagged Mvb12-GFP (upper panels) or Vps23-6HA (lower panels) and plasmids for the expression of wild-type or mutant forms of Vps37-myc were immunoprecipitated with anti-myc antiserum. Coprecipitating proteins were resolved by SDS-PAGE and analyzed by western blotting with mAbs to HA, myc, or GFP as indicated. Immunoprecipitates from cells expressing wild-type *VPS23* (D) or *VPS37* (F) were loaded at 5× (D) or 2× (F) reduced levels relative to immunoprecipitates from cells expressing empty vector or mutant proteins to compare relative levels of copurifying proteins despite differences in the stability of the mutant complexes. Bar = 2 μM.

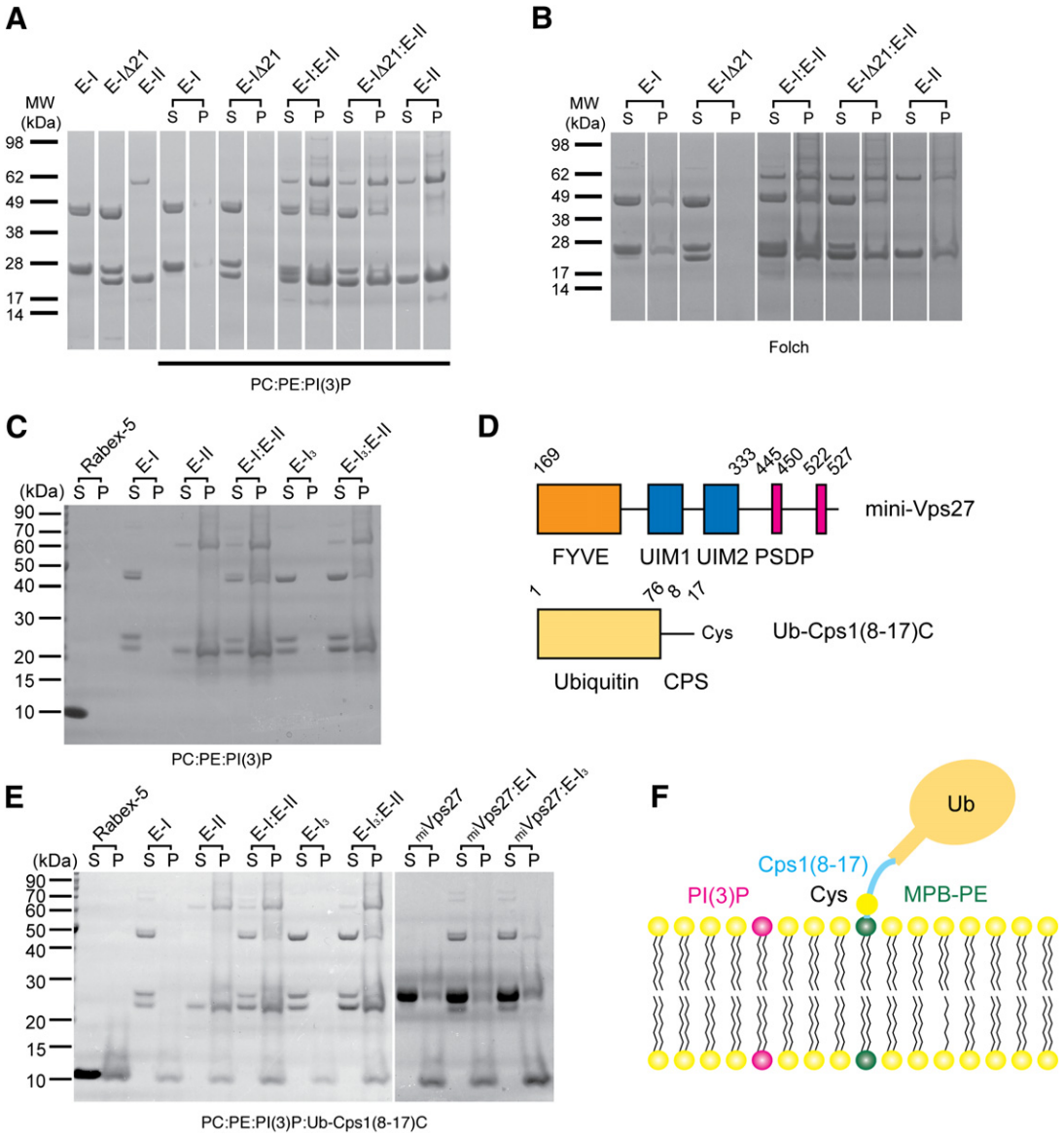

Figure 6. Sedimentation of ESCRT-I with Model Liposomes In Vitro

(A) ESCRT-I has a weak intrinsic ability to bind to synthetic PI(3)P-containing liposomes that depends on the N-terminal helix of Vps37. ESCRT-II binds strongly to these liposomes and recruits ESCRT-I in vitro independent of the Vps37 N-terminal helix.

(B) ESCRT-I sediments with brain liposomes, indicating the interaction with the N-terminal helix, does not require PI(3)P. ESCRT-I Vps37 Δ1-21 does not bind to brain liposomes, showing that the stalk and headpiece do not bind lipids.

(C) The triple ESCRT-I complex with the Vps37 Δ1–21 deletion (EI_3) is compared to intact ESCRT-I for binding to synthetic PI(3)P-containing liposomes. Both complexes are recruited to the same extent by ESCRT-II.

(D) Schematic of Mini-Vps27 and Ub-Cps1(8–17)C Constructs.

(E and F) Sedimentation with ubiquitin-Cps1 linker-conjugated synthetic PI(3)P-containing liposomes, schematized in (F). ESCRT-II and mini-Vps27 bind to these liposomes. ESCRT-I and triple ESCRT-I do not bind in the absence of other complexes but bind strongly in the presence of ESCRT-II and more weakly in the presence of mini-Vps27.

heterotetramer structure. Known structures of the yeast Vps23 UEV (Teo et al., 2004b) and Vps28 C-terminal domains (Pineda-Molina et al., 2006), together with the heterotetrameric core presented here, represent 88% of the mass of the complex, missing only flexible loops linking the UEV and Vps28 C-terminal domains and functionally nonessential extensions from the termini of Vps37 and Mvb12. Hydrodynamic analyses show that the UEV and Vps28 C-terminal domains are in an open conformation, constrained only by their fully flexible tethers to the core. This core-and-appendage organization is familiar in other contexts such as the adaptor protein-2 complex (Collins

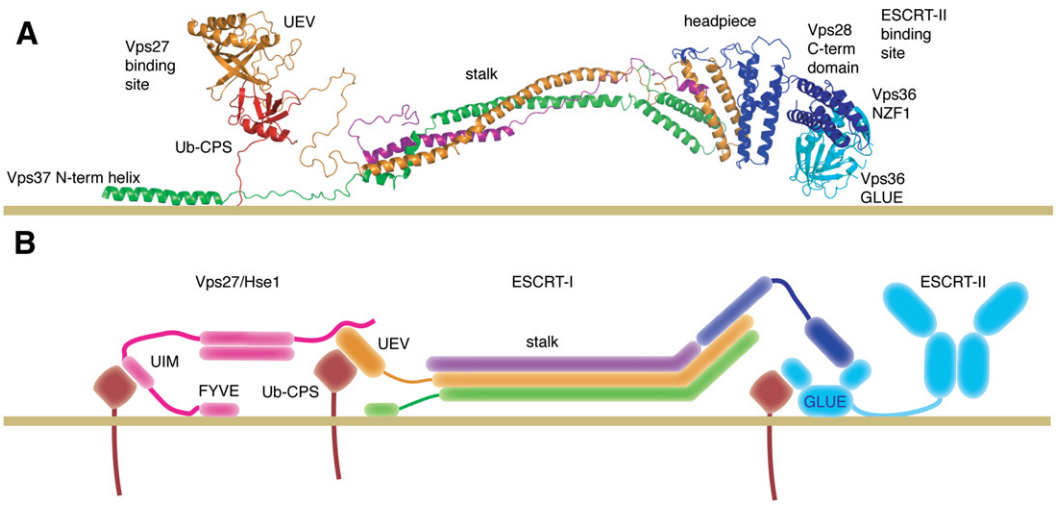

Figure 7. Membrane-Docked Model for ESCRT-I

(A) Structural model for yeast ESCRT-I docked to an endosomal membrane. The GLUE domain (PDB code 2CAY) (Teo et al., 2006) and NZF1 domain of ESCRT-II (PDB code 2J9U) (Gill et al., 2007) are cyan, ubiquitinated Cps1 is red, and ESCRT-I subunits are colored as in Figures 2–4.

(B) Schematic diagram of the docked model, incorporating simplified models of the interacting Vps27/Hse1 and ESCRT-II complexes.

et al., 2002). The combination of crystallographic analysis of the core and domains separately with hydrodynamic analysis illustrates the power of hybrid structural methodology to address challenging structural problems.

A Structural Model for ESCRT-I on the Membrane

In order to model ESCRT-I bound to an endosomal membrane, we inventoried its physical interactions with the membrane. Consistent with a lack of known phosphoinositide-binding domains, we found that ESCRT-I binds acidic phospholipids to a modest extent, but does not bind specifically to PI(3)P (Figures 6A and 6B). The highly basic N-terminal 21 amino acids of Vps37, which are absent in the crystallized construct, are required for the weak binding to acidic phospholipids in vitro, although they are not essential for ESCRT-I function and localization in vivo (not shown). When ESCRT-I and full-length ESCRT-II are mixed, ESCRT-I associates tightly with PI(3)P-containing liposomes. However, the interaction with ESCRT-II is insufficient to target ESCRT-I in vivo in the absence of Vps27, even though it can do so in vitro. We also found that ESCRT-I can assemble with model cargo and a model Vps27 protein on PI(3)P-containing liposomes in the absence of ESCRT-II. The model Vps27 used is less potent than ESCRT-II at recruiting ESCRT-I in vitro, which may reflect the limitations of the model system.

The orientation of ESCRT-I on the endosomal membrane can be inferred from the heterotetramer core structure, the known interactions of the UEV and Vps28 C-terminal domains, and the Vps37 N-terminal helix interaction with membranes. The ubiquitination of the ESCRT-I substrate Cps1 11 residues from the start of its transmembrane helix shows that the UEV domain is capable of functional ubiquitin binding very near the membrane. The NZF1 zinc finger, which is inserted within the split GLUE domain of the ESCRT-II subunit Vps36, binds to the ESCRT-I Vps28 C-terminal domain, while the GLUE domain itself binds to membrane-embedded PI(3)P (Teo et al., 2006). This dictates proximity of the Vps28 C-terminal domain to the membrane. The interaction between the Vps37 basic N-terminal segment and acidic phospholipids suggests that this part of the complex also contacts the membrane. Taken together, these constraints align the stalk roughly parallel to the plane of the membrane (Figure 7).

Function of the Stalk

The stalk is formed by three of the four subunits of ESCRT-I, and within these three subunits, residues that participate in intersubunit contacts were selected for mutagenesis. Mutations within the triple-helical stalk region of Mvb12 or Vps23 reduced the assembly of Mvb12 into the ESCRT-I complex and led to sorting defects similar to those of cells lacking Mvb12. Simultaneous mutation of two different regions of the Vps23 stalk appears to destabilize the entire ESCRT-I complex by disrupting the association of Vps23 with both Vps37 and Mvb12, accounting for the abrogation of sorting of all cargo tested. Taken together, the Vps23 and Mvb12 mutant data show that the integrity of the stalk is important for the stability and assembly of the complex. However, mutation of Vps37 at the base of the stalk had only mild effects on the stability and assembly of ESCRT-I subunits, yet still disrupted the sorting of CPY, Ste3, and Sna3. This result implicates the stalk in cargo sorting independent of its roles in ESCRT-I stability or assembly.

The postulate that Mvb12 has a central role in organizing ESCRT-I structure begs the question as to why the

phenotype of *mvb12* is milder than that of other ESCRT-I subunits. Mvb12 is not essential for headpiece assembly (Kostelansky et al., 2006; Teo et al., 2006) and has only one clear-cut function: to increase the stability of the stalk. Vps23 and Vps37 are as important for stalk formation as Mvb12, but in contrast to Mvb12, they are also required for headpiece assembly, which is in turn required to integrate Vps28 into the complex. The solution structure of heterotrimeric ESCRT-I in the absence of Mvb12 is still extended, although it is not as extended as intact ESCRT-I, and it is destabilized as judged by limited proteolysis (Kostelansky et al., 2006). The presence of some residual extended structure in the absence of Mvb12 is consistent with the residual function and stability of ESCRT-I in the absence of Mvb12. The stalk regions of yeast Vps23 and Vps37 are conserved in their human orthologs (Figures 3E, S3, and S4). Human Vps23 (Tsg101) and Vps37B/C are required for HIV budding on the basis of knockdown studies (Garrus et al., 2001; Eastman et al., 2005), and mutations within the triple coiled-coil and hybrid regions of human Vps23 block budding of HIV (Martin-Serrano et al., 2003). There is thus likely to be a human counterpart to Mvb12, although its identity is unclear. Thus the stalk is a structurally and functionally conserved feature of ESCRT-I from yeast to humans.

Function of Mvb12

While this paper was under review, three other laboratories reported the identification of Mvb12 as an ESCRT-I component (Curtiss et al., 2006; Oestreich et al., 2006; Chu et al., 2006;). Each of these three reports emphasizes a different biological function for Mvb12. Babst and coworkers note that Mvb12 is required for the efficient recycling of ESCRT-I from membranes in addition to its role in sorting (Curtiss et al., 2006). Katzmann's group suggests a cargo-selective role for Mvb12 based on their observation that trafficking defects in *mvb12Δ* cells are more severe for some cargo than others (Oestreich et al., 2006). Two major models have been put forward to account for the differential effects of *mvb12* deletion on various cargo (Curtiss et al., 2006; Oestreich et al., 2006). In the first, Mvb12 has a direct cargo-selective adaptor role, while in the second model, cargo-dependent defects reflect the existence of two or more partially separate MVB pathways. At this stage, there are no data to decisively favor one model over the other, and this is an important area for further study.

Emr and coworkers have proposed that Mvb12 promotes trimerization of soluble ESCRT-I in yeast cytosol and that its biological function is to inhibit the ESCRT-I/ESCRT-II interaction (Chu et al., 2006). However, the soluble form of ESCRT-I is a monomer of 1:1:1:1 subunit stoichiometry, not a trimer (Figures 2 and S2; Table S2). We found that Mvb12 does not affect the binding of ESCRT-I/ESCRT-II to membranes, and Williams and coworkers found that Mvb12 has no effect on the affinity of ESCRT-I for ESCRT-II in solution (Gill et al., 2007). This is consistent with our structural finding that the Vps28 C-terminal domain, which binds to ESCRT-II, does not interact with Mvb12 and is therefore unlikely to be regulated by Mvb12. Taken together, the available data argue against the concept that Mvb12 has as its main function the direct regulation of ESCRT-I/ESCRT-II binding. Instead, the accumulated biological, biochemical, and structural data on Mvb12 are most consistent with a model in which it is an integral component of the core structure of ESCRT-I whose main role is to stabilize the stalk.

Membrane trafficking is an inherently mechanical process. Rigid rod- and stalk-like molecules are omnipresent in trafficking pathways. The coiled-coil stalk structures in proteins such as EEA1 (Dumas et al., 2001) are oriented normal to membranes and tether vesicles to each other or to organelles. Elongated structures in membrane-binding and -coat proteins are oriented parallel to the membrane surface. The elongated BAR domains of proteins such as amphiphysin contact the membrane directly (Peter et al., 2004), while the clathrin leg is part of a scaffold that organizes membrane-bound structures without contacting the membrane directly (Brodsky et al., 2001; Kirchhausen, 2000). The docked model of ESCRT-I places the stalk parallel to the plane of the membrane, but not in direct contact with it. In this model, the stalk spatially organizes interactions at the membrane by imposing physical restrictions on their distances relative to each other, yet does not contact the membrane directly.

Lumenal vesicles in yeast multivesicular bodies have a mean diameter of 24 nm (Nickerson et al., 2006). Several ESCRT pathway components have rigid, elongated structures whose lengths are of the same order of magnitude as the lumenal vesicles themselves. These include the ESCRT-I core at 18 nm, ESCRT-II at 15 nm (Hierro et al., 2004; Teo et al., 2004a), and the Bro1 domain at 10 nm (Kim et al., 2005). Strikingly, although perhaps coincidentally, the maximum dimension of intact ESCRT-I in solution is ~25 nm, remarkably close to the mean diameter of a yeast MVB luminal vesicle. A key role for the stalk is most consistent with a function for ESCRT-I as a sophisticated machine acting in coordination with other rigid, elongated ESCRT components.

Conclusion

We have developed a comprehensive structural model for the intact ESCRT-I complex with a number of ramifications for ESCRT function. Our results favor a model in which Mvb12 is an integral component of ESCRT-I. The UEV and Vps28 C-terminal domains have substantial freedom to diffuse in search of their interaction partners, restricted only by their tethers. This structural model is consistent with the lack of any observed effect of Mvb12 on the binding of ESCRT-I to membranes, ubiquitin, Vps27, or ESCRT-II in vitro. ESCRT-I interacts only weakly with membranes and ubiquitin and is thus not recruited to endosomes in the absence of targeting by Vps27. The observation that all ESCRT ubiquitin-binding domains interact with the same Ile-44 patch on ubiquitin led to the "hand-off" model in which ESCRT complexes

sequentially bind to cargo (reviewed by Hurley and Emr, 2006). The structure shows that a rigid stalk holds the ESCRT-I and ESCRT-II ubiquitin-binding sites too far apart for direct hand off, strongly arguing against hand off between ESCRT-I and II. We favor an alternative model in which an assembly of multiple ESCRT complexes simultaneously binds to multiple ubiquitinated cargo molecules. The structure of the trimeric ESCRT-I headpiece (Kostelansky et al., 2006; Teo et al., 2006) revealed a globular 6 nm structure consistent with a simple role as an assembly hub, linking domains that bound cargo and other ESCRT complexes. We now find that the core is nearly 18 nm long and the intact complex is ~25 nm long. It is difficult to rationalize the evolution of such an elongated structure merely to assemble the subunits. The shape and size of ESCRT-I favor a model in which ESCRT-I directly participates in regulating mechanical aspects of cargo recruitment and membrane remodeling.

EXPERIMENTAL PROCEDURES

Fluorescence Microscopy

Wild-type and mutant strains expressing chromosomally integrated Mvb12-GFP or Vps23-GFP were labeled with FM4-64 and viewed by double-label fluorescence microscopy of fixed cells. Uptake of 40 μM FM4-64 by live cells was performed at 30°C for 1 hr, after which cells were resuspended in YPD and incubated for 1 hr at 30°C. Cells were washed twice in 1M Tris pH 8.0 containing 1% sodium azide and 1% sodium fluoride before imaging. Live and fixed cells were imaged with a 100× oil-immersion objective on a Zeiss Axioplan2 fluorescence microscope, and images were captured with a CoolSnap camera using MetaMorph software and adjusted using Adobe Photoshop.

Coprecipitation Experiments and Western Blotting

Log phase cells were converted to spheroplasts and stored at −70°C (Conibear and Stevens, 2002). For immunoprecipitation of Vps23, spheroplasts from either 20 OD_{600} or 100 OD_{600} of cells were resuspended in 1 ml of lysis buffer (600 mM sorbitol, 20 mM HEPES at pH 7.2, 50 mM KCl, 100 mM potassium acetate, 1% TX-100). Lysates were incubated with 2 μl of either rabbit anti-HA antiserum or rabbit anti-myc antiserum for 1 hr at 4°C and then with protein G sepharose (Amersham) for 1 hr at 4°C. The pellets were washed three times in 20 mM HEPES at pH 7.2 and 50 mM KCl and subjected to SDS-PAGE. Coprecipitated proteins were detected by western blotting with monoclonal antibodies to HA (HA.11, Covance Research Products), GFP (Roche scientific), or myc (4A6, Upstate) followed by HRP-labeled anti-mouse secondary antibody (Jackson ImmunoResearch or Sigma). Blots were developed with enhanced chemiluminescence and either exposed to film (X-OMAT LS, Kodak), or luminescent images were captured with a Fluor-S MAX MultiImager and analyzed using Quantity One software.

Crystal Structure Determination

Crystals of the ESCRT-I heterotetramer were grown at 21°C by hanging drop vapor diffusion mixing 2 μl of 4 mg/ml protein in 50 mM Tris (pH 7.4), 150 mM NaCl, 5 mM DTT with an equal volume of 100 mM citric acid (pH 4.0), and 800 mM ammonium sulfate. Phases were calculated by combining a 3.6 Å two wavelength SeMAD data set with multiple isomorphous replacement data from 3.0 Å gold and platinum derivative data sets. The structure was refined against a 2.7 Å native data set, as described in the Supplemental Data.

Hydrodynamic Modeling

All calculations of hydrodynamic properties from structural coordinates were carried out using Hydropro (Garcia de la Torre et al., 2000). Details of the procedure are described in the Supplemental Data.

Liposome-Binding Experiments

Liposomes used for this study are as follows: Folch fraction (Sigma), 80% POPC:20% POPE (Avanti Polar Lipids), 77% POPC:20% POPE: 3% PI(3)P (Echelon), 77% POPC:15% POPE: 5% MPB-PE (1,2-dipalmitoyl-*sn*-glycero-3-phosphoethanolamine-*N*-[4-(*p*-maleimidophenyl)butyramide]; Avanti Polar Lipids):3% PI(3)P. The liposomes were prepared at a total lipid concentration of 1 mg/ml by evaporating the solvent from the desired lipid mixture using a nitrogen stream. The dried lipids were resuspended in 150 μl of 0.3 M sucrose, and the solution was incubated at room temperature under nitrogen for 1 hr with periodic vortexing; 1 ml of water was added, and the sample was sedimented in an ultracentrifuge at 17,000 × g for 30 min at 4°C. The supernatant was removed, and the pellet was frozen and thawed three times using liquid nitrogen to break up large particles. The pellet was dissolved in 1 ml of buffer A (10 mM HEPES at pH 7.4 and 150 mM NaCl) and extruded 15 times through a 0.1 μm filter. To chemically conjugate Ub-Cps1(8–17)C to the liposome (77% POPC:15% POPE: 5% MPB-PE: 3% PI[3]P), 450 μg of Ub-Cps1(8–17)C was added to 850 μl of 1 mg/ml solution of total lipids and incubated at room temperature for 3 hr. The supernatant was removed by sedimentation at 128,000 × g at 4°C for 1 hr, washed with 1 ml of the buffer A, and sedimented for 1 hr. The pellet was resuspended in 850 μl of the buffer A.

For binding experiments, 50 μg of the liposomes were mixed with 50 μg of protein and were brought up to a total volume of 200 μl with buffer A, incubated at room temperature for 30 min, and sedimented at 128,000 × g at 4°C for 30 min. The pellet was washed once with 200 μl of the buffer A and again sedimented for 30 min. Samples of the supernatant (15 μl) and pellet were analyzed by SDS-PAGE. As a control for ubiquitin binding, the tandem A20 ZnF-MIU domain construct of Rabex-5 was used (Lee et al., 2006). This Rabex-5 construct runs on SDS-PAGE at the same position as lipid-conjugated Ub-Cps1(8–17)C, but binding is clearly visualized by an increase in the intensity of the Coomassie blue-stained band. To further confirm that the lipid-conjugated Ub-Cps1(8–17)C was functional, surface plasmon resonance experiments were carried out with liposomes bound to an L-1 chip using a Biacore T-100 instrument. Rabex-5 A20 ZnF-MIU bound with 10 μM affinity (S.L. and J.H.H., unpublished), consistent with previous surface plasmon resonance analysis using immobilized GST ubiquitin (Lee et al., 2006).

Supplemental Data

Supplemental Data include five figures, four tables, Supplemental Experimental Procedures, and Supplemental References and can be found with this article online at http://www.cell.com/cgi/content/full/129/3/485/DC1/.

ACKNOWLEDGMENTS

We thank A. Hierro for preparing ESCRT-II, S. Horte and M. Davey for technical advice and assistance, R. Piper and S. Emr for plasmids, Y. Ye and J. Bonifacino for comments on the manuscript, and G. Hummer for discussions. J.H.H. thanks S. Emr for exchanging unpublished information. Use of the advanced photon source was supported by the U S Department of Energy, Basic Energy Sciences, Office of Science, under Contract No.W-31-109-Eng-38. This research was supported by NIH intramural support, NIDDK and IATAP (J.H.H.) and funding from the Canadian Institutes of Health Research, the BC Research Institute for Children's & Women's Health, and the Michael Smith Foundation for Health Research (E.C.). M.S.K. is a PRAT fellow of the NIGMS, NIH.

Received: November 21, 2006
Revised: February 12, 2007
Accepted: March 7, 2007
Published online: April 19, 2007

REFERENCES

Babst, M. (2005). A Protein's Final ESCRT. Traffic *6*, 2–9.

Bilodeau, P.S., Urbanowski, J.L., Winistorfer, S.C., and Piper, R.C. (2002). The Vps27p-Hse1p complex binds ubiquitin and mediates endosomal protein sorting. Nat. Cell Biol. *4*, 534–539.

Bilodeau, P.S., Winistorfer, S.C., Kearney, W.R., Robertson, A.D., and Piper, R.C. (2003). Vps27-Hse1 and ESCRT-I complexes cooperate to increase efficiency of sorting ubiquitinated proteins at the endosome. J. Cell Biol. *163*, 237–243.

Bonangelino, C.J., Chavez, E.M., and Bonifacino, J.S. (2002). Genomic screen for vacuolar protein sorting genes in Saccharomyces cerevisiae. Mol. Biol. Cell *13*, 2486–2501.

Bowers, K., and Stevens, T.H. (2005). Protein transport from the late Golgi to the vacuole in the yeast Saccharomyces cerevisiae. Biochimica Et Biophysica Acta-Molecular Cell Research *1744*, 438–454.

Brodsky, F.M., Chen, C.Y., Knuehl, C., Towler, M.C., and Wakeham, D.E. (2001). Biological basket weaving: Formation and function of clathrin- coated vesicles. Annu. Rev. Cell Dev. Biol. *17*, 517–568.

Chu, T., Sun, J., Saksena, S., and Emr, S.D. (2006). New component of ESCRT-I regulates endosomal sorting complex assembly. J. Cell Biol. *175*, 815–823.

Collins, B.M., McCoy, A.J., Kent, H.M., Evans, P.R., and Owen, D.J. (2002). Molecular architecture and functional model of the endocytic AP2 complex. Cell *109*, 523–535.

Conibear, E. (2002). An ESCRT into the endosome. Mol. Cell *10*, 215–216.

Conibear, E., and Stevens, T.H. (2002). Studying yeast vacuoles. In Guide To Yeast Genetics And Molecular And Cell Biology, Pt *C*, 408–432.

Curtiss, M., Jones, C., and Babst, M. (2006). Efficient cargo sorting by ESCRT-I and the subsequent release of ESCRT-I from multivesicular bodies requires the subunit Mvb12. Mol. Biol. Cell *18*, 636–645.

Demirov, D.G., and Freed, E.O. (2004). Retrovirus budding. Virus Res. *106*, 87–102.

Dumas, J.J., Merithew, E., Sudharshan, E., Rajamani, D., Hayes, S., Lawe, D., Corvera, S., and Lambright, D.G. (2001). Multivalent endosome targeting by homodimeric EEA1. Mol. Cell *8*, 947–958.

Eastman, S.W., Martin-Serrano, J., Chung, W., Zang, T., and Bieniasz, P.D. (2005). Identification of human VPS37C, a component of endosomal sorting complex required for transport-I important for viral budding. J. Biol. Chem. *280*, 628–636.

Garcia de la Torre, J., Huertas, M.L., and Carrasco, B. (2000). Calculation of hydrodynamic properties of globular proteins from their atomic-level structure. Biophys. J. *78*, 719–730.

Garrus, J.E., von Schwedler, U.K., Pornillos, O.W., Morham, S.G., Zavitz, K.H., Wang, H.E., Wettstein, D.A., Stray, K.M., Cote, M., Rich, R.L., et al. (2001). Tsg101 and the vacuolar protein sorting pathway are essential for HIV-1 budding. Cell *107*, 55–65.

Gavin, A.C., Aloy, P., Grandi, P., Krause, R., Boesche, M., Marzioch, M., Rau, C., Jensen, L.J., Bastuck, S., Dumpelfeld, B., et al. (2006). Proteome survey reveals modularity of the yeast cell machinery. Nature *440*, 631–636.

Gill, D.J., Teo, H., Sun, J., Perisic, O., Veprintsev, D.B., Emr, S.D., and Williams, R.L. (2007). Structural insight into the ESCRT-I/-II link and its role in MVB trafficking. EMBO J. *26*, 600–612.

Hicke, L., Schubert, H.L., and Hill, C.P. (2005). Ubiquitin-binding domains. Nat. Rev. Mol. Cell Biol. *6*, 610–621.

Hierro, A., Sun, J., Rusnak, A.S., Kim, J., Prag, G., Emr, S.D., and Hurley, J.H. (2004). Structure of the ESCRT-II endosomal trafficking complex. Nature *431*, 221–225.

Hurley, J.H., and Emr, S.D. (2006). The ESCRT complexes: structure and mechanism of a membrane-trafficking network. Annu. Rev. Biophys. Biomolec. Struct. *35*, 277–298.

Hurley, J.H., Lee, S., and Prag, G. (2006). Ubiquitin binding domains. Biochem. J. *399*, 361–372.

Katzmann, D.J., Babst, M., and Emr, S.D. (2001). Ubiquitin-dependent sorting into the multivesicular body pathway requires the function of a conserved endosomal protein sorting complex, ESCRT-I. Cell *106*, 145–155.

Katzmann, D.J., Odorizzi, G., and Emr, S.D. (2002). Receptor downregulation and multivesicular-body sorting. Nat. Rev. Mol. Cell Biol. *3*, 893–905.

Katzmann, D.J., Stefan, C.J., Babst, M., and Emr, S.D. (2003). Vps27 recruits ESCRT machinery to endosomes during MVB sorting. J. Cell Biol. *162*, 413–423.

Kim, J., Sitaraman, S., Hierro, A., Beach, B.M., Odorizzi, G., and Hurley, J.H. (2005). Structural basis for endosomal targeting by the Bro1 domain. Dev. Cell *8*, 937–947.

Kirchhausen, T. (2000). Clathrin. Annu. Rev. Biochem. *69*, 699–727.

Kostelansky, M.S., Sun, J., Lee, S., Kim, J., Ghirlando, R., Hierro, A., Emr, S.D., and Hurley, J.H. (2006). Structural and functional organization of the ESCRT-I trafficking complex. Cell *125*, 113–126.

Krogan, N.J., Cagney, G., Yu, H.Y., Zhong, G.Q., Guo, X.H., Ignatchenko, A., Li, J., Pu, S.Y., Datta, N., Tikuisis, A.P., et al. (2006). Global landscape of protein complexes in the yeast Saccharomyces cerevisiae. Nature *440*, 637–643.

Lee, S., Tsai, Y.C., Mattera, R., Smith, W.J., Kostelansky, M.S., Weissman, A.M., Bonifacino, J.S., and Hurley, J.H. (2006). Structural basis for ubiquitin recognition and autoubiquitination by Rabex-5. Nat. Struct. Mol. Biol. *13*, 264–271.

Martin-Serrano, J., Zang, T., and Bieniasz, P.D. (2003). Role of ESCRT-I in retroviral budding. J. Virol. *77*, 4794–4804.

Morita, E., and Sundquist, W.I. (2004). Retrovirus budding. Annu. Rev. Cell Dev. Biol. *20*, 395–425.

Nickerson, D.P., West, M., and Odorizzi, G. (2006). Did2 coordinates Vps4-mediated dissociation of ESCRT-III from endosomes. J. Cell Biol. *175*, 715–720.

Oestreich, A.J., Davies, B.A., Payne, J.A., and Katzmann, D.J. (2006). Mvb12 is a novel member of ESCRT-I involved in cargo selection by the multivesicular body pathway. Mol. Biol. Cell *18*, 646–657.

Peter, B.J., Kent, H.M., Mills, I.G., Vallis, Y., Butler, P.J.G., Evans, P.R., and McMahon, H.T. (2004). BAR domains as sensors of membrane curvature: The amphiphysin BAR structure. Science *303*, 495–499.

Pineda-Molina, E., Belrhali, H., Piefer, A.J., Akula, I., Bates, P., and Weissenhorn, W. (2006). The crystal structure of the C-terminal domain of Vps28 reveals a conserved surface required for Vps20 recruitment. Traffic *7*, 1007–1016.

Pornillos, O., Alam, S.L., Davis, D.R., and Sundquist, W.I. (2002). Structure of the Tsg101 UEV domain in complex with the PTAP motif of the HIV-1 p6 protein. Nat. Struct. Biol. *9*, 812–817.

Shih, S.C., Katzmann, D.J., Schnell, J.D., Sutanto, M., Emr, S.D., and Hicke, L. (2002). Epsins and Vps27p/Hrs contain ubiquitin-binding domains that function in receptor endocytosis. Nat. Cell Biol. *4*, 389–393.

Slagsvold, T., Aasland, R., Hirano, S., Bache, K.G., Raiborg, C., Trambaiano, D., Wakatsuki, S., and Stenmark, H. (2005). Eap45 in mammalian ESCRT-II binds ubiquitin via a phosphoinositide-interacting GLUE domain. J. Biol. Chem. *280*, 19600–19606.

Slagsvold, T., Pattni, K., Malerod, L., and Stenmark, H. (2006). Endosomal and non-endosomal functions of ESCRT proteins. Trends Cell Biol. *16*, 317–326.

Sundquist, W.I., Schubert, H.L., Kelly, B.N., Hill, G.C., Holton, J.M., and Hill, C.P. (2004). Ubiquitin recognition by the human TSG101 protein. Mol. Cell *13*, 783–789.

Teo, H., Perisic, O., Gonzalez, B., and Williams, R.L. (2004a). ESCRT-II, an endosome-associated complex required for protein sorting: Crystal structure and interactions with ESCRT-III and membranes. Dev. Cell *7*, 559–569.

Teo, H., Veprintsev, D.B., and Williams, R.L. (2004b). Structural insights into endosomal sorting complex required for transport (ESCRT-I) recognition of ubiquitinated proteins. J. Biol. Chem. *279*, 28689–28696.

Teo, H.L., Gill, D.J., Sun, J., Perisic, O., Veprintsev, D.B., Vallis, Y., Emr, S.D., and Williams, R.L. (2006). ESCRT-I core and ESCRT-II GLUE domain structures reveal role for GLUE in linking to ESCRT-I and membranes. Cell *125*, 99–111.

Accession Numbers

Coordinates have been deposited in the protein data bank with accession code 2P22.